AGU PUBLICATIONS

JGR

Journal of Geophysical Research: Space Physics

RESEARCH ARTICLE
10.1002/2015JA022010

Key Points:
- Whistlers are observed in 80% of data at predicted satellite locations
- About 22.9% of the RBSP whistlers are related with a possible WWLLN source lightning
- About 40.1% more of coincident whistlers are found if source regions are extended

Correspondence to:
H. Zheng,
haozheng@uw.edu

Citation:
Zheng, H., R. H. Holzworth, J. B. Brundell, A. R. Jacobson, J. R. Wygant, G. B. Hospodarsky, F. S. Mozer, and J. Bonnell (2016), A statistical study of whistler waves observed by Van Allen Probes (RBSP) and lightning detected by WWLLN, *J. Geophys. Res. Space Physics*, *121*, doi:10.1002/2015JA022010.

Received 8 OCT 2015
Accepted 16 FEB 2016
Accepted article online 18 FEB 2016

©2016. American Geophysical Union. All Rights Reserved.

A statistical study of whistler waves observed by Van Allen Probes (RBSP) and lightning detected by WWLLN

Hao Zheng[1], Robert H. Holzworth[1], James B. Brundell[2], Abram R. Jacobson[1], John R. Wygant[3], George B. Hospodarsky[4], Forrest S. Mozer[5,6], and John Bonnell[6]

[1]Earth and Space Sciences, University of Washington, Seattle, Washington, USA, [2]UltraMSK, Dunedin, New Zealand, [3]Physics and Astronomy, University of Minnesota, Minneapolis, Minnesota, USA, [4]Physics and Astronomy, University of Iowa, Iowa City, Iowa, USA, [5]Physics Department, University of California, Berkeley, California, USA, [6]Space Sciences Laboratory, University of California, Berkeley, California, USA

Abstract Lightning-generated whistler waves are electromagnetic plasma waves in the very low frequency (VLF) band, which play an important role in the dynamics of radiation belt particles. In this paper, we statistically analyze simultaneous waveform data from the Van Allen Probes (Radiation Belt Storm Probes, RBSP) and global lightning data from the World Wide Lightning Location Network (WWLLN). Data were obtained between July to September 2013 and between March and April 2014. For each day during these periods, we predicted the most probable 10 min for which each of the two RBSP satellites would be magnetically conjugate to lightning producing regions. The prediction method uses integrated WWLLN stroke data for that day obtained during the three previous years. Using these predicted times for magnetic conjugacy to lightning activity regions, we recorded high time resolution, burst mode waveform data. Here we show that whistlers are observed by the satellites in more than 80% of downloaded waveform data. About 22.9% of the whistlers observed by RBSP are one-to-one coincident with source lightning strokes detected by WWLLN. About 40.1% more of whistlers are found to be one-to-one coincident with lightning if source regions are extended out 2000 km from the satellites footpoints. Lightning strokes with far-field radiated VLF energy larger than about 100 J are able to generate a detectable whistler wave in the inner magnetosphere. One-to-one coincidences between whistlers observed by RBSP and lightning strokes detected by WWLLN are clearly shown in the L shell range of $L = 1–3$. Nose whistlers observed in July 2014 show that it may be possible to extend this coincidence to the region of $L \geq 4$.

1. Introduction

Previous observations of energetic electron flux indicate that the Earth's radiation belts are distributed in two distinct zones separated by a region of depleted flux called the slot [e.g., *Horne et al.*, 2003, Figure 2]. The structure of the inner zone ($L < 2$) tends to be relatively stable, in comparison to the outer zone ($L \geq 3$), which is highly dynamic [*Millan and Thorne*, 2007]. Over the past few decades, it has been shown that this difference is primarily related to the source and loss mechanisms that control radiation belt electrons. It is believed that in the inner magnetosphere, pitch angle scattering (including both Coulomb collisions and resonant scattering by whistler mode waves) controls the loss of energetic electrons [*Abel and Thorne*, 1998a, 1998b]. Coulomb collisions with atmospheric constituents are the dominant loss process for energetic electron ($E \geq 100$ keV) inside $L = 1.3$ [*Walt and MacDonald*, 1964; *Abel and Thorne*, 1998a]. Above $L = 1.3$, the long-term energetic electron population is largely controlled by whistler mode waves, including plasmaspheric hiss, lightning-generated whistlers, and man-made transmitter signals. The calculations in *Abel and Thorne* [1998a] suggest that all three types of whistler mode waves may play important roles in the loss of energetic electrons, but different types of whistler mode waves may interact with different electron energies and be dominant at different L shells. Specifically, the lightning-generated whistlers, which are the concern of this work, are suggested to become important at $L = 2.0$, provide the dominant scattering process at $L = 2.4$ and still make a contribution at $L = 3.2$ [*Abel and Thorne*, 1998a]. Recent studies have also shown that whistler mode chorus wave can provide local acceleration of energetic electrons by efficient energy diffusion in the outer radiation belts [e.g., *Summers et al.*, 2002; *Meredith et al.*, 2003; *Li et al.*, 2014]. It has also been shown that intense whistler mode chorus emission may cause microburst electron precipitation into the atmosphere [*Thorne et al.*, 2005].

Previous studies have shown that whistlers play an important role in the dynamics of the radiation belts and are partly responsible for the loss of the energetic electrons [e.g., *Dungey*, 1963; *Voss et al.*, 1984, 1998; *Abel and Thorne*, 1998a, 1998b; *Lauben et al.*, 2001; *Rodger et al.*, 2004; *Millan and Thorne*, 2007; *Meredith et al.*, 2009]. Pitch angle scattering of energetic Van Allen belt electrons by whistlers can result in the precipitation of these electrons into the atmosphere [*Dungey*, 1963]. Lightning-induced electron precipitation (LEP) from the Earth's radiation belts, caused by whistler wave-particle interaction, is a known troposphere-to-magnetosphere coupling mechanism. The first satellite measurements of LEP events were obtained as a result of the SEEP experiment on S81-1 satellite [*Voss et al.*, 1984]. By using the same data, *Voss et al.* [1998] found that a single LEP burst (10^{-3} erg s^{-1} cm^{-2}) in the slot region is estimated to deplete ~0.001% of the particles in the region. Whistlers can be important for pitch angle diffusion of 100–250 keV electrons in the $2 < L < 3$ range [*Voss et al.*, 1998]. *Rodger et al.* [2004] provide evidence for the relative significance of the electron losses driven by whistler-induced electron precipitation and that caused by VLF transmitters. Magnetospherically reflected whistlers generated by lightning are also considered to be a source of plasmaspheric hiss [*Sonwalkar and Inan*, 1989]. By using ray-tracing simulations, it was shown that whistlers produced by a single lightning flash, but entering the magnetosphere at different points, can form a continuous hiss-like signal at a fixed point [*Draganov et al.*, 1992]. The analysis of DE-1 and IMAGE data showed that the geographic distribution of hiss over the ~500 Hz to ~3 kHz frequency range is similar to the geographic distribution of lightning strokes [*Green et al.*, 2005]. Similar results are shown in the analysis of CRRES data for the plasmaspheric hiss at higher frequencies $f > 2$ kHz [*Meredith et al.*, 2006].

Plasmaspheric electron densities are an important and fundamental parameter in the dynamics of Earth's radiation belts. The propagation of whistlers in the plasmasphere is strongly connected with cold electron density. Whistler data from ground-based stations were used to identify the large-scale electron-density irregularities in the plasmasphere [*Park and Carpenter*, 1970] and also to present a statistical study of equatorial plasmaspheric electron density and associated flux tube electron content [*Park et al.*, 1978]. Understanding the link between lightning activities and whistler observations on satellites may assist in estimating of plasmaspheric electron densities and testing of magnetospheric models of electron density and energy distribution [*Liemohn and Scarf*, 1964].

The broadband radio waves produced by lightning discharge, called "sferics," can propagate in the Earth-ionosphere waveguide and be detected thousands of kilometers away from the source. A portion of the sferics can penetrate into the ionosphere, coupling with the whistler mode in the very low frequency (VLF) band, and travel upward obliquely within tens of degrees along the geomagnetic field line [*Helliwell*, 1965]. The source and the destination of lightning-generated whistlers have been studied for years. Early in situ rocket-borne measurements demonstrated the one-to-one connection between whistlers observed in the upper atmosphere/ionosphere and individual lightning strokes from specific thunderstorms within 1000–2000 km [e.g., *Holzworth et al.*, 1985, 1999; *Kelley et al.*, 1990; *Li et al.*, 1991]. SCATHA satellite VLF data indicated that whistlers are rarely detected near the magnetic equator across the L shells of $L = 5.5–9.0$ [*Koons*, 1985]. The apparent scarcity of whistlers near geostationary altitude as covered by the SCATHA satellite, suggests that there may be few if any propagation paths from the Earth-ionosphere waveguide to the outer regions of magnetosphere. But it also may indicate that VLF spectral data are not always investigated with high enough time resolution to easily detect lightning whistlers. *Gurnett and Inan* [1988] examined the data from the DE spacecraft and discovered several lightning whistlers up to 15 kHz or even 25 kHz at $L < 4$ [*Gurnett and Inan*, 1988, Figures 21–23]. *Holzworth et al.* [1999] used a global three-dimensional two-fluid code to investigate the propagation of whistlers at 0.5, 1, and 2.0 kHz into the high-latitude magnetosphere. The results show that with southward interplanetary magnetic field, the energy of whistlers which start from magnetic latitude above 70° can propagate to near magnetopause or high-altitude magnetosphere.

In recent decades, localized and global ground lightning detection networks have been gradually improving, which has proven critical in linking whistlers to their source lightning strokes. *Santolík et al.* [2009] analyzed three lightning strokes detected by METEORAGE, sferics received by Nançay station, and the corresponding whistlers observed by the DEMETER satellite at 707 km altitude. The electric field data and optical flashes measurements on the C/NOFS satellite were used with simultaneous global lightning location information from WWLLN in *Holzworth et al.* [2011] to show that whistlers have abundant access to the ionosphere, even close to the magnetic equator. Both papers showed that the one-to-one coincidence between whistler waves observed at LEO and individual lightning strokes and the penetration into the topside ionosphere occurs at nearly vertical wave vector angles due to the gradient of electron density. *Fiser et al.* [2010] used two

reference samples to automatically detect the fractional hop whistlers on the DEMETER satellite. A local lightning detection network in Europe was used to match the lightning and whistler data. They found that the amplitudes of whistlers decrease monotonically with horizontal distance up to ~1000 km from the source lightning and the amplitude of whistlers are stronger at nighttime than during the daytime.

In this paper, we will explore the connection between lightning sferics and whistlers by using data from the Van Allen Probes (formerly known as the Radiation Belt Storm Probes (RBSP)) and World Wide Lightning Location Network (WWLLN). The high-resolution waveform data obtained near the geomagnetic equator provide a wider area coverage in the inner magnetosphere than LEO satellites like DEMETER. Global lightning data, including the location, time, and energy for every individual stroke, are simultaneously collected in the conjunction periods. One-to-one coincidences between whistlers observed by RBSP and lightning strokes detected by WWLLN are explored in this work.

2. RBSP and WWLLN

The RBSP satellites were launched in August 2012 into a near-equatorial orbit with 10° inclination, apogee altitude of 30,050–31,250 km (~5.8 R_E from the center of the Earth) and perigee altitude of 500–675 km [*Stratton et al.*, 2013]. These constraints place the satellites in orbits that cut through both the inner and outer radiation belts. After launch the satellites were officially renamed to the Van Allen Probes. The fundamental purpose of the RBSP mission is to provide a better understanding of the processes that drive changes within the Earth's radiation belts. The Electric Field and Waves (EFW) instrument [*Wygant et al.*, 2013] on the RBSP can provide both 3-D electric field and 3-D magnetic field waveform data. The burst mode data we used in this work have a sampling rate of 16.4 ksamples s^{-1}. Another instrument called RBSP-EMFISIS (The Electric and Magnetic Field Instrument Suite and Integrated Science) [*Kletzing et al.*, 2013] can also provide 3-D electric and magnetic field waveform data with a sampling rate of 35 ksamples s^{-1} in 6 s blocks. The burst mode of EMFISIS can be trigged automatically or manually.

WWLLN is a global very low frequency lightning-location system using the time-of-group-arrival (TOGA) technique [*Dowden et al.*, 2002]. It can detect both cloud-to-ground (CG) and intracloud (IC) lightnings, but the type of lightning is not distinguished in the data. At present, WWLLN includes over 70 participating stations. This network improves in accuracy and detection efficiency with increased number of stations. The number of lightning strokes located increased from 10.6 million to 28.1 million (~165%) when the number of WWLLN stations increased from 11 in 2003 to 30 in 2007 [*Rodger et al.*, 2009]. As of 2011 the network had an estimated detection efficiency of about 11% for CG lightning over the continental United States, and the number can increase to >30% for higher peak current lightning [*Hutchins et al.*, 2012]. Knowledge of individual stroke locations, with high temporal and spatial accuracy, is very helpful for studying VLF energy radiation and the global electric circuit [e.g., *Hutchins et al.*, 2013, 2014].

This paper presents data collected during two periods of conjunction work, from July to September 2013 and from March to April 2014, during which we were able to collect specific burst mode RBSP data. The conjunction work of 2013 between WWLLN and RBSP began on 1 July 2013 and ended on 15 September 2013. The following study period started on 15 March 2014 and ended on 30 April 2014. For each day of the two time periods, a prediction was computed in advance, to determine the best times to collect the broadband wave data. Burst mode sampling was conducted during the predicted time for each satellite. In addition to the statistical study conducted in this work, we also provide some examples from other burst mode sampling intervals when high L shell whistlers were seen.

2.1. Prediction

Due to the limit of data storage onboard and in agreement with the RBSP instrument team, the burst mode for this lightning study at 16.4 ksamples/s on RBSP-EFW was limited to 10 min per day per satellite (in 2014, only RBSP-B was available for the data collection). Additionally, due to data download limitations, everyday we had to select 3 or 4 min out of the 10 min stored broadband data, which were then downloaded. In order to predict the best 10 min/d to collect high sampling rate burst mode data on RBSP satellites, we traced the satellite magnetic footpoints over a lightning occurrence map. The footpoints data were calculated at an altitude of 100 km using the T89c magnetic field model developed by *Tsyganenko* [1989] and is provided by the SSC 4D Orbit Viewer from NASA (http://sscweb.gsfc.nasa.gov/tipsod/). This lightning occurrence map is composed of all global WWLLN lightning data from the same date in the last 3 years (2010–2012). That is, we used 3 weeks of data, 1 week from each of the last 3 years, centered at the day of the year for which we want a prediction. This

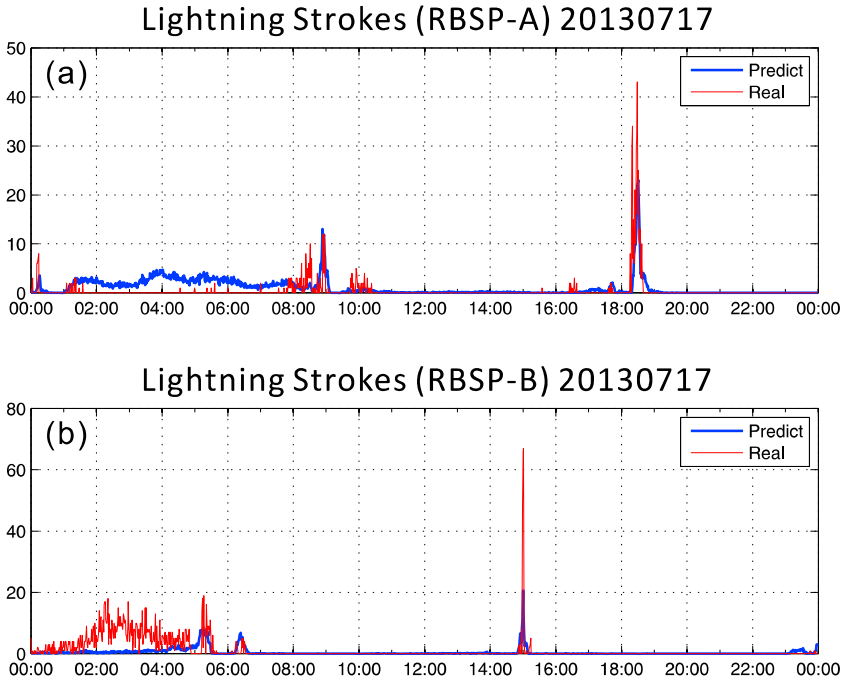

Figure 1. Prediction and real results for (a) RBSP-A and (b) RBSP-B on 17 July 2013. The red lines show the real result, and blue lines show the prediction result.

map therefore had global lightning data from 21 days. We then used the predicted satellite ephemeris with 1 min time resolution to identify the magnetic field footpoints in both Northern and Southern Hemispheres. From previous research [*Santolík et al.*, 2009; *Fiser et al.*, 2010; *Holzworth et al.*, 2011], we know that the entry point of whistlers into the ionosphere can be thousands of kilometers away from the source lightning. In our work, a source area of 20° × 20° box was used in the prediction instead of a circle with ~1000 km radius in order to get a faster calculation in the program. Although the area of 20° × 20° box is not the same at different latitudes, the predicted peaks will not change significantly because the results are dominated by the variance of lightning occurrence rate at different latitudes. In our prediction, for every 1 min footpoint location, we summed all lightning strokes within the 20° × 20° box centered at the footpoint. This gave us a 1 min resolution prediction of possible strokes at the magnetic footpoint for the whole day. Figures 1a and 1b show the prediction results for RBSP-A and RBSP-B on 17 July 2013 as an example. The blue lines represent the prediction result using WWLLN data from 2010 to 2012 and the red lines represent the real lightning number in the same footpoint box using actual WWLLN data on 17 July 2013. The time difference between prediction peak and actual peak is within 5 min for both satellites. If this example is true in general, it would suggest that if we set a time period with ±5 min centered at the predicted peak time, there should be lightning strokes detected around the footpoints within the predicted 10 min. The conjunction work between WWLLN and RBSP started in July 2013 after the prediction test for the whole month of June was finished. For RBSP-A and RBSP-B, 93.3% and 96.7% of daily time shifts between actual peak and prediction peak are within 5 min. Even on days when the time difference between the actual and predicted peaks is larger than 5 min, there are still many lightning strokes detected during the predicted 10 min period. After the RBSP burst mode sampling on the satellites was finished, we checked the actual WWLLN lightning stroke numbers detected within the 20° × 20° box for every 1 min footpoint location and selected the best 3–4 min to download everyday.

2.2. Dechirping

Figure 2 shows a 1 s spectrogram and waveform plot of the RBSP-A observation on 17 July 2013 during 18:27:20.5–18:27:21.5 UT period. Figure 2a shows the power spectral density (PSD) of B_u component (*UVW* coordinate system is the spacecraft coordinate system, where the *W* axis is the spin axis and is orthogonal to *U* and *V* axis). In Figure 2a, at least five intense whistler events are detected and identified by numbered oblique arrows. There are also some weak events shown as unnumbered vertical arrows in Figure 2a. The original waveform data of B_u is shown in Figure 2c. Figure 2e shows the lightning strokes detected by WWLLN in the 20° × 20° box centered at the footpoint. The lightning strokes detected in the first half second are shown

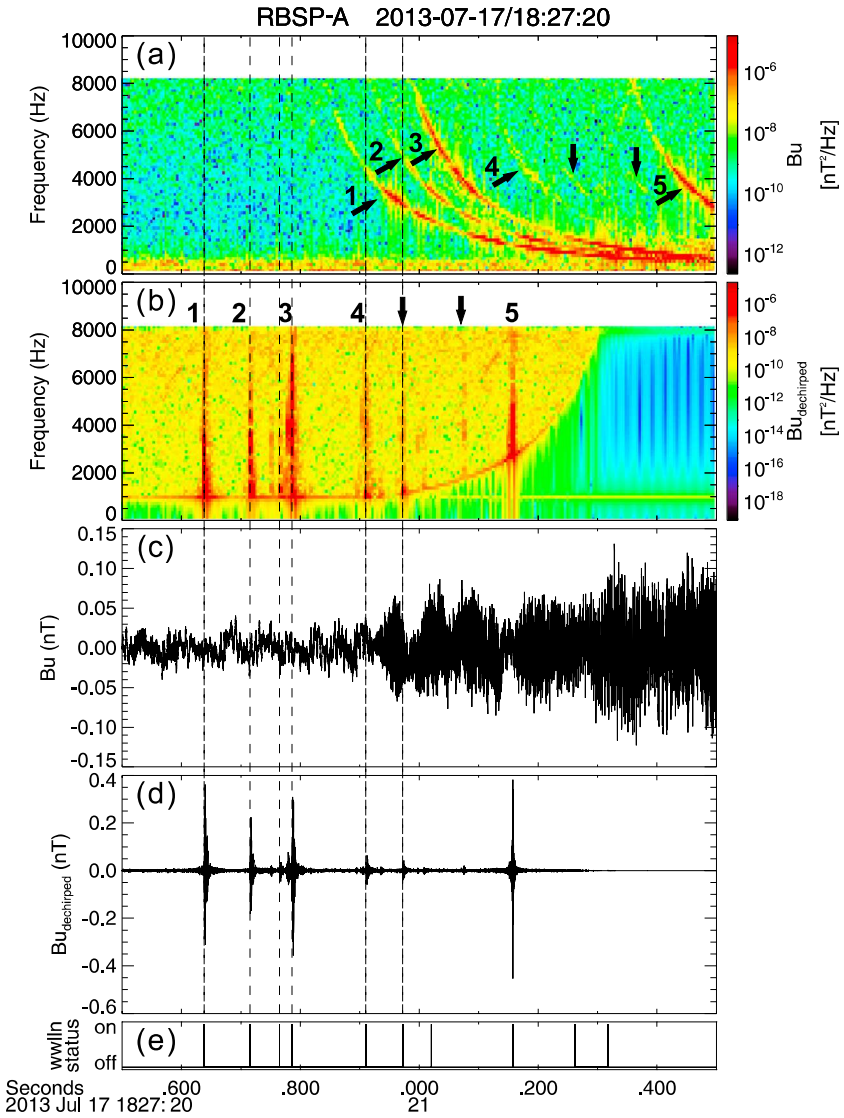

Figure 2. Spectrogram and waveform of Bu component on RBSP-A from 18:27:20.5 UT to 18:27:21.5 UT on 17 July 2013. (a) Original spectrogram. (b) Dechirped spectrogram. (c) Original waveform. (d) Dechirped waveform. (e) Timing of WWLLN lightning strokes near the satellite footpoints. The vertical dashed lines represent the WWLLN lightning time observed in first half of the second.

as dashed vertical lines in Figures 2a–2d. From the original data (Figures 2a and 2c), it is difficult to determine whether there is an actual one-to-one coincidence between the lightning detected by WWLLN and whistlers observed by RBSP-A or if they are actually unrelated events that happened to be observed simultaneously. In the ionosphere at low latitude and midlatitudes, the time delay of a whistler approximately varies as $\frac{D}{\sqrt{f}}$, where f is the wave frequency and D is the dispersion constant. *Jacobson et al.* [2011] developed an automated algorithm called "dechirping" for recognizing and selecting the signatures of electron whistlers observed on C/NOFS satellite. Here we employ this method to identify the best dispersion constant between 0 and 400 $s^{1/2}$ in each analysis window (detailed definition described in *Jacobson et al.*, 2011, section 4.1 and equation (1)). In the final step, we shift different frequency parts of waveform back to the arrival time by using the best fit to $\frac{D}{\sqrt{f}}$ for each time interval. Figures 2b and 2d are the dechirped results for the data in Figures 2a and 2c. In Figure 2b, the whistlers detected in Figure 2a have been corrected for the time delay and are no longer dispersed. Instead, the whistler energy is now sharpened in the vertical red bars between 1 kHz and 8 kHz. In order to reduce the contribution of noise below the waveguide cutoff and alias effects around the Nyquist frequency, low (1 kHz) and high (8 kHz) cutoff frequencies were applied before the dechirping process. After the dechirping process, the vertical dashed lines (WWLLN lightning time) and vertical red bars

(dechirped whistler time) are located quite close in time. The dechirping method enables us to identify even low-intensity whistlers from background noise. The two weak signals in Figure 2a (vertical arrows) become much more prominent in Figure 2b (also vertical arrows). The dechirping process also makes it possible to identify overlapping whistlers. Using the number 3 whistler in Figure 2a as an example, we see it contains two to three whistler traces observed at almost the same time. In Figure 2d, the number 3 event clearly resolves as several independent dechirped whistler packets which are shown in the dechirped waveform. Considering the leftward migration of signal energy in the dechirping, a 50% overlap between the time windows was applied. We only compared the lightning strokes and dechirped peaks in the first half second because the dechirped peak near the end of the observation window may not be accurate since only the high-frequency packet of whistler waveform underwent the dechirping process. In Figure 2, all six lightning strokes (in first 0.5 s) detected in the 20° × 20° box centered at the footpoints correspond to whistler signals observed by RBSP-A. The correspondence between number 5 whistler and WWLLN lightning stroke is also good and can be identified in the next time window. There is still a small time difference between the dechirped waveform peak and WWLLN lightning time because we have not yet accounted for the propagation time.

2.3. Propagation Model

WWLLN provides lightning stroke location with better than 15 μs temporal accuracy and 10 km spatial accuracy [*Jacobson et al.*, 2006]. We assume that the VLF sferics generated from lightning strokes propagate in the Earth-ionosphere waveguide to the footpoint of satellites with a speed slightly less than c [*Dowden et al.*, 2002] (where c is the speed of light in a vacuum). Near the footpoint they couple with the plasma and propagates obliquely along the geomagnetic field to the RBSP satellites according to the oblique whistler dispersion relation. This type of propagation process has been used extensively in previous work [e.g., *Holzworth et al.*, 1999; *Jacobson et al.*, 2011]. It is based on the quasi-longitudinal approximation to the Appleton-Hartree dispersion relation [*Helliwell*, 1965].

To compare the WWLLN lightning stroke time with the dechirped peak time from RBSP, we subtract two terms from the dechirped peak time. The first is the speed of light propagation time along the geomagnetic field line from the footpoint to the satellites. Here we used IGRF-11 model in the Geopack DLM to trace the geomagnetic field and calculated the length of the geomagnetic field line. The second term is the propagation time in the Earth-ionosphere waveguide from WWLLN lightning stroke to the footpoint of RBSP satellites. After subtracting the two terms on the dechirped peak time, the whistler is effectively transported back to the possible candidate of source lightning. We call it the "corrected" dechirped peak time in this paper.

2.4. One-to-One Coincidence Between WWLLN and RBSP

The goal of this paper is to find possible one-to-one coincidences between lightning and whistlers by comparing the WWLLN lightning time and corrected dechirped peak time from RBSP. For all the continuous burst mode data, we divided B_u component into several analysis windows. Each window includes 16,384 samples (1 s) and 50% overlapping (8196 samples). Every 1 s window was then extended to a 2 s window by adding another 16,384 empty data just before the B_u data, in order to leave enough space for the leftward migration of the signal during the dechirping process. Every new 2 s window was fed into the dechirping process, and all dechirped peaks between 1 s and 1.5 s were saved for later analysis except for the first and last window (the dechirped peaks of first and last window were searched from 0 s to 1.5 s and from 1 s to 2 s, respectively). Once there was at least one dechirped peak found in the analysis window, we loaded the WWLLN lightning data detected in the same 2 s analysis window as the source candidates for the dechirped peaks. At the same time, the footpoint with shorter arc distance (spherical distance between one of the footpoint to lightning location) to each lightning stroke was selected from two hemispheres and used to correct the dechirped peak. The time differences between source lightning candidates and corrected dechirped peaks in the same analysis window were calculated, and the histogram results are shown in Figure 3. We have already shown that the time difference between WWLLN lightning and dechirped peak is usually a few milliseconds in Figure 2, so only time differences between −100 ms and 100 ms are plotted here. Figure 3a shows a histogram of the time difference between corrected dechirped peak and WWLLN lightning ($t_{\text{corrected}} - t_{\text{WWLLN}}$) in 1 ms bin, for all stroke locations. Figures 3b and 3c are similar but only include WWLLN stroke locations within 10,000 km and 2000 km away from the nearest footpoint. In Figures 3a–3c, a clear peak of match numbers is located between −30 ms and 0. There are several possible reasons for the time difference. The first reason is the uncertainty of the dispersion constant. Take a whistler observed on 5 August 2013 as an example. In the 236th analysis window with a dispersion constant of 220.5 $s^{1/2}$, the dechirped peak was located at 20:00:58.748679.

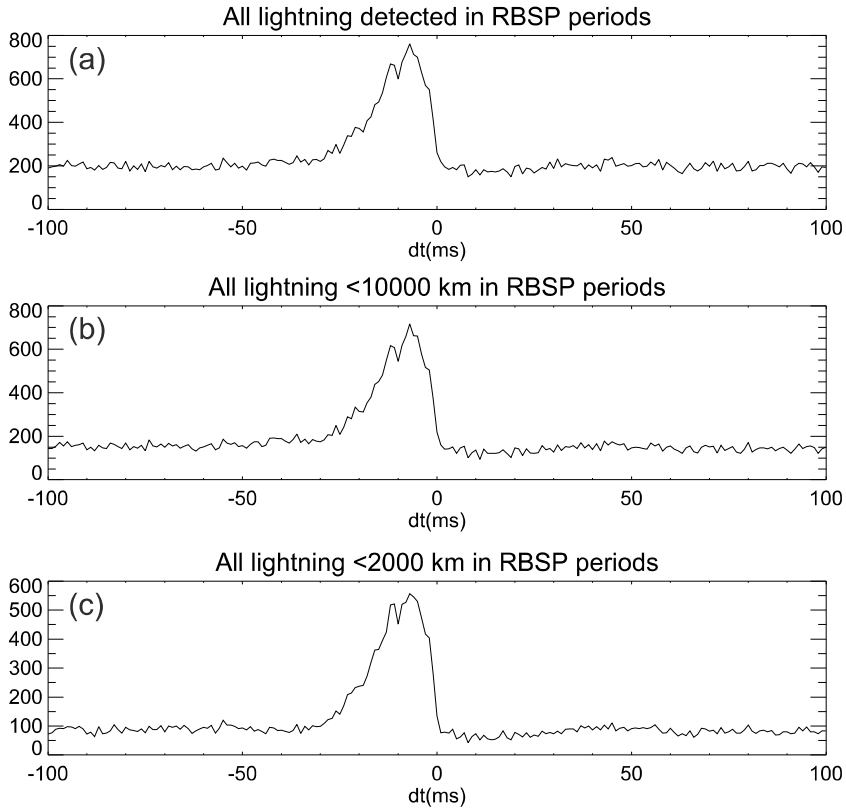

Figure 3. Histogram of corrected dechirped peak time minus WWLLN stroke time in every 2 s dechirping window, after correction for two propagation terms. (a) Including all WWLLN strokes. (b) Including WWLLN strokes within 10,000 km. (c) Including WWLLN strokes within 2000 km.

(This peak was located in the 1.5 s to 2 s of 236th window, so it was not saved here but would be saved in the 237th window.) While in the 237th analysis window with a dispersion constant of 208.0 $s^{1/2}$, the same peak was located at 20:00:58.761069 instead (12.39 ms difference). The second reason is the uncertainty of two subtracted propagation terms. Waveguide and field line arc lengths are calculated from models, which also generated errors. Finally, the errors may be introduced by the propagation model, since it may not work perfectly for all latitudes (L shells).

The maximum absolute value of time difference above the "noise" level between corrected dechirped peak and its WWLLN source was found to be around 30 ms in Figure 3. By using this number, an automatic one-to-one coincidence search was applied to the whole data set. For every dechirped peak, we loaded global WWLLN lightning data, corrected the dechirped peak time, and then found the one-to-one coincidence with time difference from −30 ms to 0.

3. Statistical Results

During the conjunction work in 2013, we downloaded 192 min over 65 separate days from RBSP-A and 192 min over 66 days from RBSP-B. In 2014, we downloaded 221 min over 39 days only from RBSP-B. In total, we collected 605 min of data across 170 distinct days for RBSP-A and RBSP-B. In July 2013, no special selection criteria was used, so the burst mode period was biased toward the low-latitude region, where lightning is most prevalent. For the highly eccentric RBSP orbit, low satellite altitude always corresponds to low L shell. Figure 2 in *Rodger et al.* [2004] showed that the lightning activity may reach to the high L shell region in the summer of the Northern Hemisphere. From August 2013 to September 2013, the prediction was changed to focus on the footpoints region with geographic latitude larger than 40°, which is poleward of the regions with highest lightning activities.

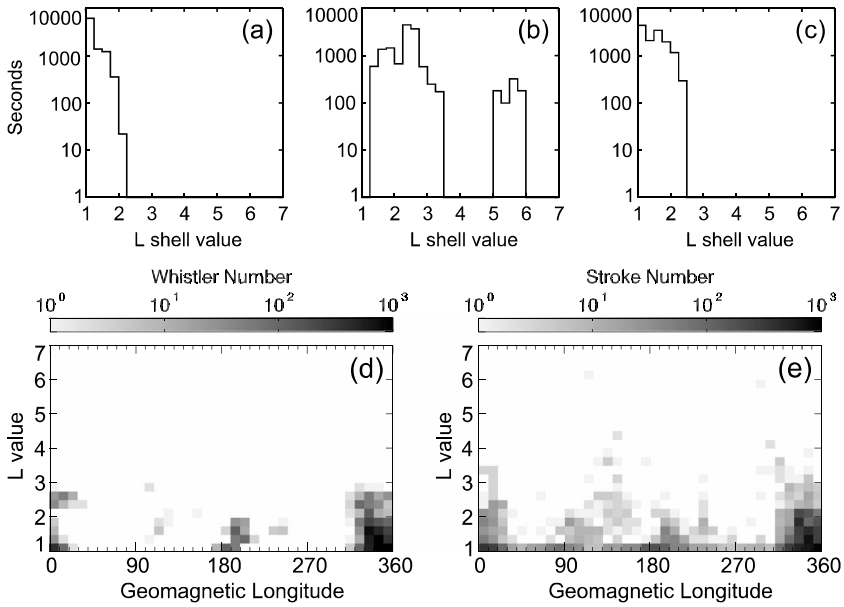

Figure 4. (a–c) L shell value distribution of data downloaded by both RBSP-A and B in seconds: (a) July 2013, (b) August and September 2013, and (c) March and April 2014. (d) Footpoint location of RBSP satellites when whistlers are observed with a one-to-one coincident WWLLN source lightning. (e) Location of WWLLN lightning strokes which are one-to-one coincident with whistlers observed on RBSP satellites. Figures 4d and 4e are all plotted in geomagnetic coordinate system.

Figure 4 shows the L shell coverage of RBSP data used in our work. As mentioned before, the burst mode sampling period is only requested when it includes the peak number of strokes in the daily prediction. For July 2013, the best prediction time occurred when the satellites were conjugate to low-latitude regions where lightning is most prevalent (Figure 4a). Thus, during the first period (July 2013), whistler observations were only made at low L shells. Beginning in August 2013, our focus shifted to the region with geographic latitude larger than 40°. In August and September 2013, the L shell values of satellite footpoints were therefore significantly higher than in July 2013 (Figure 4b). Most of the data in this period were sampled between $L = 2$ and 3. There are 780 s (13 min) of data sampled at $L \geq 5$ region. In March and April 2014, the L shell value coverage returned to $L < 2.5$ due to the seasonal change of global lightning (Figure 4c). Figure 4d shows the global coverage of the satellites footpoints when whistlers were observed by RBSP satellites. All of the dechirped peaks are observed inside of $L = 3$. The data mainly cover four regions, with three small portions located at 100°–130°, 170°–220°, and 230°–250°, and a large region located at 310°–40°. These are approximately corresponding to Europe/Africa, Asian, Oceania, and America, respectively. In Figure 4d, the longitude coverage is limited in several parts because lightning has a higher occurrence rate on continents than over oceans. Figure 4e shows the distribution of lightning strokes that are one-to-one coincident with whistlers observed by RBSP satellites. Figure 4d refers to the L value of the RBSP satellites during whistlers observation, while Figure 4e refers to the L value of the lightning source location. In Figure 4e, the matched lightning strokes show full coverage of all geomagnetic longitudes and have peak numbers around the same regions of dechirped peaks in Figure 4d. There are some lightning strokes at high L shell, larger than $L = 3$ in Figure 4e, which are the sources of whistlers observed by RBSP inside of $L = 3$ in the magnetosphere. This means the distance between lightning and satellite footpoint may be larger than 1000–2000 km, which is consistent with previous research [e.g., *Holzworth et al.*, 1999].

Table 1 shows the statistical results of both RBSP-A and RBSP-B. The total of 605 min data are divided into three periods: 151 min in July 2013, 233 min in August and September 2013, and 221 min in March and April 2014. Whistlers are observed in 485 min (80.2%) of data, with 140 min (92.7%), 150 min (64.4%), and 195 min (88.2%) in the three periods, respectively. A total number of 20,986 whistlers are observed by RBSP satellites. The 8308 (39.6%) of them are one-to-one coincident with WWLLN lightning strokes. Specifically, 2526/5938 (42.5%), 730/2454 (29.7%), and 5052/12,594 (40.1%) of the observed RBSP whistlers are one-to-one coincident with WWLLN lightning strokes in the three periods. In the 485 min, 206,470 lightning strokes are detected

Table 1. Statistical Results of Whistlers Observed by RBSP and WWLLN Lightning

	Jul 2013	Aug–Sep 2013	Mar–Apr 2014	Total
Number of sampling minute	151	233	221	605
Number of sampling minute with dechirped peaks	140	150	195	485
Percentage	92.7%	64.4%	88.2%	80.2%
Number of dechirped peaks	5938	2454	12,594	20,986
Number of coincident dechirped peaks	2526	730	5052	8308
Percentage	42.5%	29.7%	40.1%	39.6%
Number of global WWLLN lightning strokes	54,675	62,520	89,275	206,470
Number of coincident WWLLN lightning strokes	2526	730	5052	8308
Percentage	4.6%	1.2%	5.7%	4.0%
Number of WWLLN lightning strokes within 2000 km	12,699	6103	20,005	38,777
Number of coincident WWLLN lightning strokes within 2000 km	2004	452	3476	5932
Percentage	15.8%	7.4%	17.4 %	15.3%

by WWLLN. Four percent of them are found to be one-to-one coincident with whistlers observed on RBSP. If we narrow the lightning locations to the area within 2000 km from the footpoints, there are 38,777 lightning strokes detected in the 485 min, and 15.3% of them are one-to-one coincident with whistlers observed on RBSP.

4. Discussion

As explained in the section 1, previous studies found that whistlers play a significant role in the dynamics of the radiation belts. But the connection between source lightning strokes and subsequent whistlers in the magnetosphere has been difficult to study due to lack of simultaneous, high time resolution waveform and global lightning observations. In this paper we present a new data set that identifies the source lightning locations for specific whistlers in the inner magnetosphere with the help of WWLLN and RBSP. Unlike *Fiser et al.* [2010], the lightning data used in our work are not simply narrowed to the region near the footpoints of satellites. Additionally, we do not use reference whistlers to automatically detect whistlers since the dispersion factor may change at different regions. The final difference between two studies is the propagation of whistlers. At low altitude, the main propagation process happens in the Earth-ionosphere waveguide between footpoint and source lightnings. While in the inner magnetosphere, the whistlers travel a long path along (or within some angles of) field lines till they are observed by satellites. We did not compare the amplitude of whistlers with horizontal distance or the amplitude of whistlers between day and night, like what *Fiser et al.* [2010] did, in this paper. The propagation model used in this work is quite simple and does not include the various propagation mechanisms of whistlers in the magnetosphere. Whether whistlers are ducted or non-ducted remains an outstanding question. Although lightning is considered the only source for whistlers, the observed one-to-one coincident rate between whistlers and lightning is much less than 100%. This rate is limited by lightning detection efficiency, the strength of whistlers, and how well we understand the propagation of whistlers.

In this work, we used the WWLLN lightning location data from 2010–2012 to forecast the lightning activity along the daily trajectory of RBSP footpoints. Then we recorded the 10 min of RBSP burst mode data for the time period with peak lightning stroke counts in the 20° × 20° grid centered at the footpoint. After onboard recording, we were only able to download 3–4 min (of the daily 10 min recording). During the entire 605 min of downloaded data, whistlers are observed 80.2% of the time we predicted, suggesting that satellites should have a high probability of observing whistlers if their footpoints are located within a few thousand kilometers of an active thunderstorm. The occurrence of these high lightning activity areas can be predicted by using archival WWLLN data. We can use the results of this method to predict the occurrence of lightning-generated whistler waves in the inner magnetosphere and its related phenomena.

In the 485 min of data, 20,986 dechirped peaks are observed by RBSP satellites. 39.6% of those peaks are one-to-one coincident with a WWLLN lightning stroke. It is obvious that WWLLN does not detect the source lightning for every whistler observed by RBSP satellites. It is found that WWLLN only has a 20–40% detection efficiency for strong CG lightning (peak current larger than 55 kA) [*Rodger et al.*, 2009; *Abarca et al.*, 2010], so the

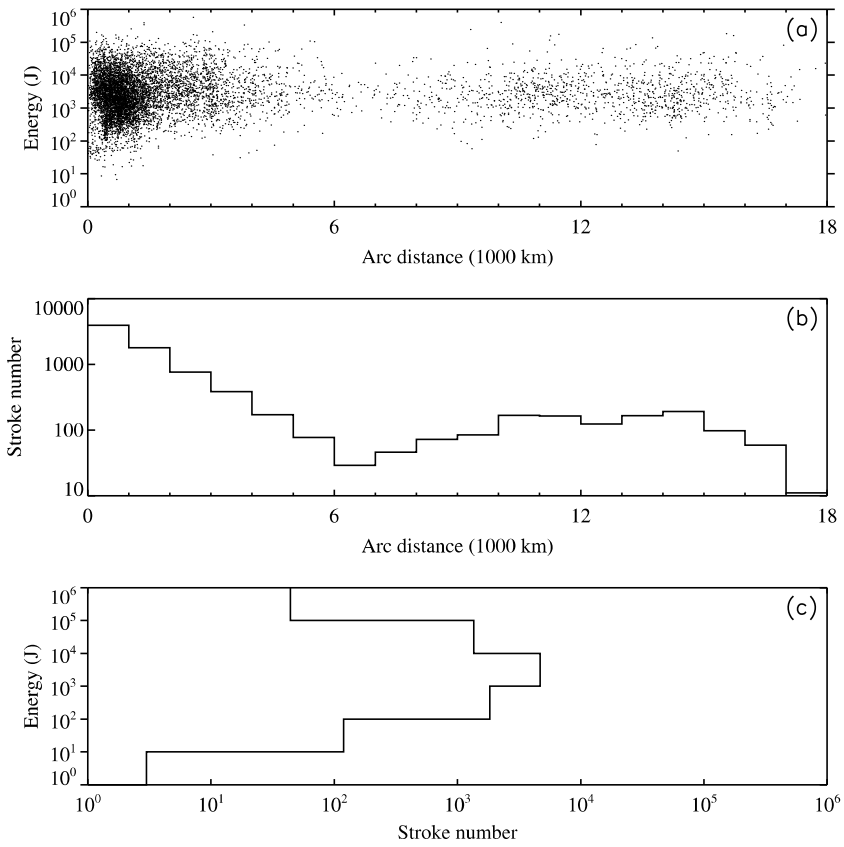

Figure 5. Distribution of one-to-one coincident lightning with energy vs arc distance from lightning to satellite footpoint. (a) Scatter plot; (b) Histogram of arc distance from lightning to satellite footpoint. (c) Histogram of lightning energy.

possible source lightning may be missed by WWLLN. A test was also undertaken to evaluate the probability that we might match whistlers with some noncorresponding lightning due to the high occurrence rate of global lightning. During the 485 min, 20 random times for every second were set as the "dechirped peaks" and fed into the same automatic one-to-one coincidence search with WWLLN lightning. The random match rate is around 16.7%. After subtracting the random match rate, we find that at least about 22.9% of whistlers correspond to a source lightning stroke detected by WWLLN. This number is comparable to the detection efficiency of WWLLN for strong lightning.

About 4.0% of WWLLN lightning strokes correspond to the whistlers observed by the RBSP satellites. Figure 5a shows the scatter plot of all the coincident WWLLN lightning strokes with energy versus arc distance in the waveguide to the nearest satellite footpoint. Figures 5b and 5c are the histograms of energy and arc distance shown in Figure 5a. In Figure 5b, we see that the number of coincident lightning strokes decreases from ~4000 with the increase of arc distance below 7000 km. Above 7000 km, the number of coincident lightning strokes shows another small peak of ~200. This phenomenon is also found in the one-to-one coincidence between WWLLN and C/NOFS data [see *Jacobson et al.*, 2011, Figure 16]. They explained it as an expected behavior of the spherical-shell effect. In Figure 5c, the energy of coincident lightning strokes shows a peak of 1–10 kJ. If we only consider the range from 50 J to 500 kJ, the average and median energy of the coincident lightning strokes are about 7.5 kJ and 2.6 kJ, respectively, while the average and median energy of all detected lightning strokes are 6.5 kJ and 2.4 kJ, respectively. *Hutchins et al.* [2012] showed that the median energy of WWLLN lightning strokes is around 2 kJ after April 2011 (see their Figure 8), which is consistent with our results. In Figure 5a, the majority of the scatter points above ~100 J may suggest that any lightning stroke with energy ≥ 100 J may generate a whistler strong enough to be detected by the RBSP-EFW. Figure 5b shows that the lightning strokes detected near the footpoints (within 7000 km) have a larger potential to generate a whistler propagated to the inner magnetosphere. In Table 1 the numbers of lightning strokes detected by WWLLN within 2000 km of footpoints (both Northern and Southern Hemispheres) are shown as 12,699, 6103,

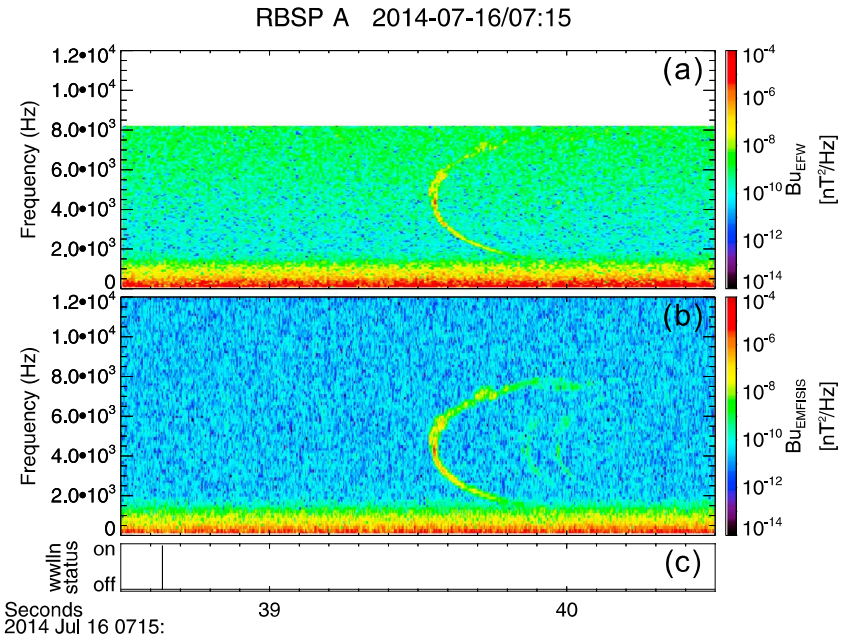

Figure 6. A nose whistler example observed by RBSP-A from 07:15:38.5 UT to 07:15:40.5 UT on 16 July 2014. (a) EFW spectrogram. (b) EMSIFIS spectrogram. (c) Timing of WWLLN lightning strokes near the satellite footpoints. The vertical dashed line also represents the WWLLN lightning time.

and 20,005 respectively. The coincident rate increased from about 4.0% to 15.3% if the source region was narrowed to within 2000 km of footpoints. If the source regions of whistlers are extended beyond 2000 km from the footpoints, the coincident whistlers can increase from 5932 to 8308 (40.1%).

We note that in August and September of 2013, the occurrence rate of one-to-one coincidence (29.7%) is much lower than in July 2013 (42.5%) or in March and April 2014 (40.1%). One reason may be that fewer lightning strokes are detected at high latitude in August and September. Although the arc distance from the possible source lightning to the footpoint varies from 0 to 18,000 km, the match rate of one-to-one coincidence between lightning and whistlers is still dominated by lightning near the footpoint especially within 2000 km. Figures 4a–4c show that the L shell coverage of the RBSP data in August and September 2013 is larger than in other two periods. The occurrence rate of lightning at high latitudes is lower than found at low latitude and midlatitude [*Hutchins et al.*, 2012], and the number of lightning strokes detected at the footpoints in August and September 2013 is lower than for the other two periods (Table 1). Another reason may be the failure of finding one-to-one coincidence between lightning and whistlers at high L shells. In Figure 4d, no dechirped peaks are observed above $L = 3$ during 7 min of data sampling between $L = 3$ and 3.5 and 13 min of data sampling above $L = 5$ in Figure 4b. This could be due to two different situations: (1) no whistlers are observed by RBSP satellites at high L shells; (2) whistlers are observed by RBSP but do not pass the dechirping process. After carefully checking the data above $L = 3$, it was found that no whistlers were observed when L is larger than 5. Although this is consistent with the work of *Koons* [1985], we cannot conclusively state that lightning has no impact at L > 5. There are three possible reasons whistlers may not be observed above $L = 5$. First, the magnetic field around the geomagnetic equator is small at high L shells, so the whistlers would have a low upper cutoff frequency and may be masked by low-frequency noise or even be reflected before they arrived at the satellites. Second, the amplitude of whistlers may be not strong enough due to the attenuation. *Burkholder et al.* [2013] showed that within the ionosphere, there is an approximately 3 order of magnitude loss of energy from the footpoint to C/NOFS satellites. Third, the propagation of whistlers at high L shell may not follow the same magnetic field line, so the lightning-generated whistler waves near the footpoint may not reach the geomagnetic equator of the same L shell. The propagation of magnetospherically reflected whistlers is studied by ray trace method, e.g., *Bortnik et al.*, 2002, 2003]. By reviewing recent EMFISIS data collected during the Northern Hemisphere summer in 2015, we identified several lightning-generated whistler waves with upper cutoff frequencies of ~2 kHz observed near the RBSP apogee ($L \approx 5.797$) which may correspond to WWLLN located lightning. It is also found that in the 7 min data located between $L = 3$ and 3.5, there

were whistlers observed by RBSP but which failed to pass the dechirping process. This may be due to the fact that the dispersion is stronger and the whistler waves may no longer be fully displayed in the 1 s window, and the dispersion constant may also exceed the number we set. At last, nose whistlers may be observed when L shell is large. Figure 6 shows an example of a nose whistler observed by RBSP-A at $L \approx 3.88$ on 16 July 2014. Lightning near the footpoint is detected at 07:15:38.64 (Figure 6c and the dashed line in Figure 6). About 0.9 s later, both EFW and EMFISIS captured the nose whistler with a nose frequency of about 4.5 kHz and an upper cutoff frequency of about 8 kHz. As shown in Figures 6a and 6b EMFISIS provides more information at high frequency (8–12 kHz). The dechirping method used in our work has a band-pass filter of 1–8 kHz, which is no longer appropriate for nose whistlers because the nose frequency is usually lower than 6 kHz or even 4 kHz in the outer magnetosphere [*Helliwell*, 1965, Figures 4–19]. With a better dechirping process in the future, we can probably get more information about the contribution of lightning to the high L shell whistlers in the magnetosphere.

5. Conclusion

A study of simultaneous observations of global lightning and whistlers was conducted from July to September 2013 and from March to April 2014. Global lightning data of the past 3 years from the WWLLN were used to forecast lightning conditions along the trajectory of RBSP's magnetic field footpoints. Ten minutes with the highest lightning probability around the footpoints were selected for burst mode recording on the satellites. Data were downloaded for short time periods during 170 days, leading to a total of 605 min of high-resolution waveform which were statistically analyzed in this paper. By using this method, lightning-generated whistlers near the magnetic equator at low L shell regions can be successfully predicted with a rate of 80.2%. This new data set should prove valuable for the future study of whistler-related phenomena. About 22.6% of the whistlers observed by the satellites correspond to possible source lightning in the actual WWLLN data, which closely matched the time and location. This rate also agrees with the detection efficiency of WWLLN. The source regions of whistlers are extended 2000 km from the footpoints in this study. About 40.1% more whistlers observed by the RBSP satellites are found to correspond with WWLLN lightning. Lightning strokes with energy larger than 100 J all have the potential to generate a whistler and propagate to the inner magnetosphere. We show that whistlers strongly correspond to WWLLN lightning at low L shell ($L < 3$) regions. The correspondence between high L shell whistlers and lightning still exist but need further study.

Acknowledgments

The authors wish to acknowledge partial support for this research from CRDF grant RUG1-7084-PA-13, from NOAA grant NA10OAR4320148, and from NSF grant 1443011. The authors wish to thank the World Wide Lightning Location Network (http://wwlln.net), a collaboration among over 50 universities and institutions, for providing the lightning location data used in this paper. The authors wish to acknowledge the Space Sciences Laboratory at University of Berkeley and the University of Minnesota for providing EFW data (data link: http://www.space.umn.edu/rbspefw-data/, PI: John Wygant) and the University of Iowa for providing the EMFISIS data (data link: http://emfisis.physics.uiowa.edu/data/index, PI: Craig Kletzing), both of which are instruments on board the Van Allen Probes.

References

Abarca, S. F., K. L. Corbosiero, and T. J. Galarneau (2010), An evaluation of the Worldwide Lightning Location Network (WWLLN) using the National Lightning Detection Network (NLDN) as ground truth, *J. Geophys. Res.*, *115*, D18206, doi:10.1029/2009JD013411.

Abel, B., and R. M. Thorne (1998a), Electron scattering loss in Earth's inner magnetosphere: 1. Dominant physical processes, *J. Geophys. Res.*, *103*(A2), 2385–2396, doi:10.1029/97JA02919.

Abel, B., and R. M. Thorne (1998b), Electron scattering loss in Earth's inner magnetosphere: 2. Sensitivity to model parameters, *J. Geophys. Res.*, *103*(A2), 2397–2407, doi:10.1029/97JA02920.

Bortnik, J., U. S. Inan, and T. F. Bell (2002), L dependence of energetic electron precipitation driven by magnetospherically reflecting whistler waves, *J. Geophys. Res.*, *107*(A8), 1150, doi:10.1029/2001JA000303.

Bortnik, J., U. S. Inan, and T. F. Bell (2003), Frequency-time spectra of magnetospherically reflecting whistlers in the plasmasphere, *J. Geophys. Res.*, *108*(A1), 1030, doi:10.1029/2002JA009387.

Burkholder, B. S., M. L. Hutchins, M. P. McCarthy, R. F. Pfaff, and R. H. Holzworth (2013), Attenuation of lightning-produced sferics in the Earth-ionosphere waveguide and low-latitude ionosphere, *J. Geophys. Res. Space Physics*, *118*, 3692–3699, doi:10.1002/jgra.50351.

Dowden, R. L., J. B. Brundell, and C. J. Rodger (2002), VLF lightning location by time of group arrival (TOGA) at multiple sites, *J. Atmos. Sol. Terr. Phys.*, *64*(7), 817–830, doi:10.1016/S1364-6826(02)00085-8.

Draganov, A. B., U. S. Inan, V. S. Sonwalkar, and T. F. Bell (1992), Magnetospherically reflected whistlers as a source of plasmaspheric hiss, *Geophys. Res. Lett.*, *19*(3), 233–236, doi:10.1029/91GL03167.

Dungey, J. (1963), Loss of Van Allen electrons due to whistlers, *Planet. Space Sci.*, *11*(6), 591–595, doi:10.1016/0032-0633(63)90166-1.

Fiser, J., J. Chum, G. Diendorfer, M. Parrot, and O. Santolik (2010), Whistler intensities above thunderstorms, *Ann. Geophys.*, *28*(1), 37–46, doi:10.5194/angeo-28-37-2010.

Green, J. L., S. Boardsen, L. Garcia, W. W. L. Taylor, S. F. Fung, and B. W. Reinisch (2005), On the origin of whistler mode radiation in the plasmasphere, *J. Geophys. Res.*, *110*, A03201, doi:10.1029/2004JA010495.

Gurnett, D. A., and U. S. Inan (1988), Plasma wave observations with the dynamics explorer 1 spacecraft, *Rev. Geophys.*, *26*(2), 285–316, doi:10.1029/RG026i002p00285.

Helliwell, R. A. (1965), *Whistlers and Related Ionospheric Phenomena*, Stanford Univ. Press, Stanford, Calif.

Holzworth, R. H., M. C. Kelley, C. L. Siefring, L. C. Hale, and J. D. Mitchell (1985), Electrical measurements in the atmosphere and the ionosphere over an active thunderstorm: 2. Direct current electric fields and conductivity, *J. Geophys. Res.*, *90*(A10), 9824–9830, doi:10.1029/JA090iA10p09824.

Holzworth, R. H., R. M. Winglee, B. H. Barnum, Y. Li, and M. C. Kelley (1999), Lightning whistler waves in the high-latitude magnetosphere, *J. Geophys. Res.*, *104*(A8), 17,369–17,378, doi:10.1029/1999JA900160.

Holzworth, R. H., M. P. McCarthy, R. F. Pfaff, A. R. Jacobson, W. L. Willcockson, and D. E. Rowland (2011), Lightning-generated whistler waves observed by probes on the Communication/Navigation Outage Forecast System satellite at low latitudes, *J. Geophys. Res.*, *116*, A06306, doi:10.1029/2010JA016198.

Horne, R. B., N. P. Meredith, R. M. Thorne, D. Heynderickx, R. H. A. Iles, and R. R. Anderson (2003), Evolution of energetic electron pitch angle distributions during storm time electron acceleration to megaelectronvolt energies, *J. Geophys. Res.*, *108*(A1), 1016, doi:10.1029/2001JA009165.

Hutchins, M. L., R. H. Holzworth, J. B. Brundell, and C. J. Rodger (2012), Relative detection efficiency of the World Wide Lightning Location Network, *Radio Sci.*, *47*, RS6005, doi:10.1029/2012RS005049.

Hutchins, M. L., R. H. Holzworth, K. S. Virts, J. M. Wallace, and S. Heckman (2013), Radiated VLF energy differences of land and oceanic lightning, *Geophys. Res. Lett.*, *40*, 2390–2394, doi:10.1002/grl.50406.

Hutchins, M. L., R. H. Holzworth, and J. B. Brundell (2014), Diurnal variation of the global electric circuit from clustered thunderstorms, *J. Geophys. Res. Space Physics*, *119*, 620–629, doi:10.1002/2013JA019593.

Jacobson, A. R., R. Holzworth, J. Harlin, R. Dowden, and E. Lay (2006), Performance assessment of the World Wide Lightning Location Network (WWLLN), using the Los Alamos Sferic Array (LASA) as ground truth, *J. Atmos. Oceanic Technol.*, *23*(8), 1082–1092, doi:10.1175/JTECH1902.1.

Jacobson, A. R., R. H. Holzworth, R. F. Pfaff, and M. P. McCarthy (2011), Study of oblique whistlers in the low-latitude ionosphere, jointly with the C/NOFS satellite and the World-Wide Lightning Location Network, *Ann. Geophys.*, *29*(5), 851–863, doi:10.5194/angeo-29-851-2011.

Kelley, M. C., J. G. Ding, and R. H. Holzworth (1990), Intense ionospheric electric and magnetic field pulses generated by lightning, *Geophys. Res. Lett.*, *17*(12), 2221–2224, doi:10.1029/GL017i012p02221.

Kletzing, C., et al. (2013), The Electric and Magnetic Field Instrument Suite and Integrated Science (EMFISIS) on RBSP, *Space Sci. Rev.*, *179*(1–4), 127–181, doi:10.1007/s11214-013-9993-6.

Koons, H. C. (1985), Whistlers and whistler-stimulated emissions in the outer magnetosphere, *J. Geophys. Res.*, *90*(A9), 8547–8551, doi:10.1029/JA090iA09p08547.

Lauben, D. S., U. S. Inan, and T. F. Bell (2001), Precipitation of radiation belt electrons induced by obliquely propagating lightning-generated whistlers, *J. Geophys. Res.*, *106*(A12), 29,745–29,770, doi:10.1029/1999JA000155.

Li, W., et al. (2014), Radiation belt electron acceleration by chorus waves during the 17 March 2013 storm, *J. Geophys. Res. Space Physics*, *119*, 4681–4693, doi:10.1002/2014JA019945.

Li, Y. Q., R. H. Holzworth, H. Hu, M. McCarthy, R. D. Massey, P. M. Kintner, J. V. Rodrigues, U. S. Inan, and W. C. Armstrong (1991), Anomalous optical events detected by rocket-borne sensor in the WIPP campaign, *J. Geophys. Res.*, *96*(A2), 1315–1326, doi:10.1029/90JA01727.

Liemohn, H. B., and F. L. Scarf (1964), Whistler determination of electron energy and density distributions in the magnetosphere, *J. Geophys. Res.*, *69*(5), 883–904, doi:10.1029/JZ069i005p00883.

Meredith, N. P., R. B. Horne, R. M. Thorne, and R. R. Anderson (2003), Favored regions for chorus-driven electron acceleration to relativistic energies in the Earth's outer radiation belt, *Geophys. Res. Lett.*, *30*(16), 1871, doi:10.1029/2003GL017698.

Meredith, N. P., R. B. Horne, M. A. Clilverd, D. Horsfall, R. M. Thorne, and R. R. Anderson (2006), Origins of plasmaspheric hiss, *J. Geophys. Res.*, *111*, A09217, doi:10.1029/2006JA011707.

Meredith, N. P., R. B. Horne, S. A. Glauert, D. N. Baker, S. G. Kanekal, and J. M. Albert (2009), Relativistic electron loss timescales in the slot region, *J. Geophys. Res.*, *114*, A03222, doi:10.1029/2008JA013889.

Millan, R., and R. Thorne (2007), Review of radiation belt relativistic electron losses, *J. Atmos. Sol. Terr. Phys.*, *69*(3), 362–377, doi:10.1016/j.jastp.2006.06.019.

Park, C. G., and D. L. Carpenter (1970), Whistler evidence of large-scale electron-density irregularities in the plasmasphere, *J. Geophys. Res.*, *75*(19), 3825–3836, doi:10.1029/JA075i019p03825.

Park, C. G., D. L. Carpenter, and D. B. Wiggin (1978), Electron density in the plasmasphere: Whistler data on solar cycle, annual, and diurnal variations, *J. Geophys. Res.*, *83*(A7), 3137–3144, doi:10.1029/JA083iA07p03137.

Rodger, C. J., R. J. McCormick, and M. A. Clilverd (2004), Testing the importance of precipitation loss mechanisms in the inner radiation belt, *Geophys. Res. Lett.*, *31*, L10803, doi:10.1029/2004GL019501.

Rodger, C. J., J. B. Brundell, R. H. Holzworth, and E. H. Lay (2009), Growing detection efficiency of the World Wide Lightning Location Network, *AIP Conf. Proc.*, *1118*(1), 15–20, doi:10.1063/1.3137706.

Santolík, O., M. Parrot, U. Inan, D. Burešová, D. Gurnett, and J. Chum (2009), Propagation of unducted whistlers from their source lightning: A case study, *J. Geophys. Res.*, *114*, A03212, doi:10.1029/2008JA013776.

Sonwalkar, V. S., and U. S. Inan (1989), Lightning as an embryonic source of VLF hiss, *J. Geophys. Res.*, *94*(A6), 6986–6994, doi:10.1029/JA094iA06p06986.

Stratton, J., R. Harvey, and G. Heyler (2013), Mission overview for the Radiation Belt Storm Probes mission, *Space Sci. Rev.*, *179*(1–4), 29–57, doi:10.1007/s11214-012-9933-x.

Summers, D., C. Ma, N. P. Meredith, R. B. Horne, R. M. Thorne, D. Heynderickx, and R. R. Anderson (2002), Model of the energization of outer-zone electrons by whistler-mode chorus during the October 9, 1990 geomagnetic storm, *Geophys. Res. Lett.*, *29*(24), 2174, doi:10.1029/2002GL016039.

Thorne, R. M., T. P. O'Brien, Y. Y. Shprits, D. Summers, and R. B. Horne (2005), Timescale for MeV electron microburst loss during geomagnetic storms, *J. Geophys. Res.*, *110*, A09202, doi:10.1029/2004JA010882.

Tsyganenko, N. (1989), A magnetospheric magnetic field model with a warped tail current sheet, *Planet. Space Sci.*, *37*(1), 5–20, doi:10.1016/0032-0633(89)90066-4.

Voss, H., et al. (1984), Lightning-induced electron precipitation, *Nature*, *312*, 740–742, doi:10.1038/312740a0.

Voss, H. D., M. Walt, W. L. Imhof, J. Mobilia, and U. S. Inan (1998), Satellite observations of lightning-induced electron precipitation, *J. Geophys. Res.*, *103*(A6), 11,725–11,744, doi:10.1029/97JA02878.

Walt, M., and W. M. MacDonald (1964), The influence of the Earth's atmosphere on geomagnetically trapped particles, *Rev. Geophys.*, *2*(4), 543–577, doi:10.1029/RG002i004p00543.

Wygant, J., et al. (2013), The electric field and waves instruments on the radiation belt storm probes mission, *Space Sci. Rev.*, *179*(1–4), 183–220, doi:10.1007/s11214-013-0013-7.